# *Gpr158* Deficiency Impacts Hippocampal CA1 Neuronal Excitability, Dendritic Architecture, and Affects Spatial Learning

Demirhan Çetereisi[1†], Ioannis Kramvis[1†], Titia Gebuis[1], Rolinka J. van der Loo[1], Yvonne Gouwenberg[1], Huibert D. Mansvelder[2], Ka Wan Li[1], August B. Smit[1] and Sabine Spijker[1*]

[1] Department of Molecular and Cellular Neurobiology, Center for Neurogenomics and Cognitive Research, Amsterdam Neuroscience, Vrije Universiteit, Amsterdam, Netherlands, [2] Department of Integrative Neurophysiology, Center for Neurogenomics and Cognitive Research, Amsterdam Neuroscience, Vrije Universiteit, Amsterdam, Netherlands

G-protein-coupled receptor 158 (*Gpr158*) is highly expressed in striatum, hippocampus and prefrontal cortex. It gained attention as it was implicated in physiological responses to stress and depression. Recently, *Gpr158* has been shown to act as a pathway-specific synaptic organizer in the hippocampus, required for proper mossy fiber-CA3 neurocircuitry establishment, structure, and function. Although rodent *Gpr158* expression is highest in CA3, considerable expression occurs in CA1 especially after the first postnatal month. Here, we combined hippocampal-dependent behavioral paradigms with subsequent electrophysiological and morphological analyses from the same group of mice to assess the effects of *Gpr158* deficiency on CA1 physiology and function. We demonstrate deficits in spatial memory acquisition and retrieval in the Morris water maze paradigm, along with deficits in the acquisition of extinction memory in the passive avoidance test in *Gpr158* KO mice. Electrophysiological recordings from CA1 pyramidal neurons revealed normal basal excitatory and inhibitory synaptic transmission, however, Schaffer collateral stimulation yielded dramatically reduced post-synaptic currents. Interestingly, intrinsic excitability of CA1 pyramidals was found increased, potentially acting as a compensatory mechanism to the reductions in Schaffer collateral-mediated drive. Both *ex vivo* and *in vitro,* neurons deficient for or with lowered levels of *Gpr158* exhibited robust reductions in dendritic architecture and complexity, i.e., reduced length, surface, bifurcations, and branching. This effect was localized in the apical but not basal dendrites of adult CA1 pyramidals, indicative of compartment-specific alterations. A significant positive correlation between spatial memory acquisition and extent of complexity of CA1 pyramidals was found. Taken together, we provide first evidence of significant disruptions in hippocampal CA1 neuronal dendritic architecture and physiology, driven by *Gpr158* deficiency. Importantly, the hippocampal neuronal morphology deficits appear to support the impairments in spatial memory acquisition observed in *Gpr158* KO mice.

**Keywords: cognition, memory, hippocampus, behavior, morphology, electrophysiology, knock out, knock down**

# INTRODUCTION

G-protein-coupled receptors (GPCRs) form a large family of seven transmembrane proteins. In the brain, these act as important regulators of synaptic transmission, neuronal excitability, and structural plasticity, through presynaptic and postsynaptic mechanisms of action (Huang and Thathiah, 2015; Leung and Wong, 2017). Several brain-expressed GPCRs were shown to modulate cognition and are suspect in the pathobiology of neuronal disorders (Catapano and Manji, 2007; Thompson et al., 2008). Collectively, GPCRs make up the largest drug target group to-date (Chan et al., 2015). Recently, G-protein coupled receptor 158 (*Gpr158*) caught attention due to its role in hippocampus-dependent memory formation via osteocalcin (OCN) signaling (Khrimian et al., 2017). *Gpr158* is found highly expressed in the brain, specifically in prefrontal regions, striatum, and hippocampus (Orlandi et al., 2012; Khrimian et al., 2017; Sutton et al., 2018). Previously, we have observed Gpr158 strongly upregulated in the hippocampus synaptic membrane fraction after stress of an immediate shock (Rao-Ruiz et al., 2015). The stress-responsiveness of *Gpr158* was further illustrated by its rapid and robust increase in expression upon glucocorticoid stimulation either *in vitro* (Patel et al., 2013), or *in vivo* (Sutton et al., 2018). Finally, *Gpr158* was shown increased in the prefrontal cortex (PFC) in the hours to days after physical stress in mice, as well as in post-mortem prefrontal tissue from depressed patients, whereas *Gpr158* KO mice exhibited resilience to unpredicted chronic mild stress (Sutton et al., 2018).

Recent work has begun shedding light on the precise function of *Gpr158* (Orlandi et al., 2012; Khrimian et al., 2017; Condomitti et al., 2018; Sutton et al., 2018). *Gpr158* overexpression in mouse medial PFC (mPFC) increases helplessness, illustrated by increased immobility in a tail-suspension (TST) and forced-swim tests (FST) (Sutton et al., 2018). On the contrary, global deletion of *Gpr158* had an anxiolytic and anti-depressant effect, exhibited by decreased immobility in TST and FST (Sutton et al., 2018). Recordings from *Gpr158* KO mPFC superficial layer pyramidals revealed increases in spontaneous excitatory postsynaptic current (sEPSC) frequency, partially supported by an increase in spine density, and an AMPA receptor (AMPAR) current-driven increase in the AMPAR/NMDAR ratio persisting regardless of dendritic spine size (Sutton et al., 2018).

Hippocampal-dependent learning appears negatively affected in *Gpr158* KO mice, as observed during Morris water maze (MWM) training, and as shown by memory deficits in the novel object recognition task (NOR) (Khrimian et al., 2017). Dentate gyrus' (DG) mossy fiber (MF) to CA3 long-term potentiation (LTP) was shown significantly impaired in these mice (Khrimian et al., 2017). Moreover, frequency and amplitude of sEPSCs, AMPAR and NMDAR evoked currents, and MF to CA3 paired pulse ratio (PPR) were all robustly reduced in *Gpr158* KO CA3 pyramidals (Condomitti et al., 2018). Although CA3 spine density and MF-CA3 synapse density were paradoxically found increased, both the area and volume per MF-CA3 synapse were robustly reduced (Condomitti et al., 2018). Importantly, the aforementioned electrophysiological and morphological deficits were pathway-specific, affecting MF to CA3 synapses, but not CA3 to CA3 association/commissural synapses. The underlying mechanism for this was elegantly demonstrated by the discovery of glypican 4 (Gpc4), which is highly enriched in MFs, as the presynaptic binding partner to postsynaptic hippocampal *Gpr158* (Condomitti et al., 2018).

Given the considerable CA1 expression from post-weaning onward (Condomitti et al., 2018; Ostrovskaya et al., 2018), as well as the role of *Gpr158* in neuronal signaling and cognition (Khrimian et al., 2017; Sutton et al., 2018), we investigated the effect of *Gpr158* deficiency on both electrophysiological properties and neuronal architecture in the hippocampus CA1 with *in vitro* and *ex vivo* approaches. We took specific advantage of measuring hippocampus-dependent behavior and performing electrophysiological recordings with cellular reconstructions in the same set of animals, allowing us to create insightful correlations between the behavior and underlying neuronal architecture observed. Taken together, our data reveal spatial learning deficits and neuronal hyperexcitability in *Gpr158* KO mice, driven by the compromised dendritic architecture of CA1 pyramidal neurons.

# MATERIALS AND METHODS

## Animals

*Gpr158* knock-out (KO) mice [$Gpr158^{TM1(KOMP)Vlcg}$] were generated by replacing the *Gpr158* gene with a LacZ cassette including a stop codon in the region of exon 1 and exon 2 (Orlandi et al., 2015), and were purchased from the KOMP repository (see **Supplementary Figure 1**). Animals were bred for >5 generations on a C57BL/6J background (Charles River, France) in the animal facility of the VU University Amsterdam. Mice were kept in standard type-2 Macrolon cages, enriched with nesting material on a 12/12 h light/dark rhythm (lights on at 7:00 AM), a constant temperature of $23 \pm 1°C$, and a relative humidity of $50 \pm 10\%$. Food and water were provided *ad libitum*. After weaning, all mice were group-housed per sex. For behavioral experiments, male mice were single-housed 1–2 weeks prior to the first test, and received a PVC tube and wooden chew stick as additional enrichment. For all behavioral experiments, we used male 8–12 weeks old *Gpr158* KO mice and wild type (WT) littermates as control, in addition to a batch of male heterozygous (HZ) *Gpr158* mice and WT littermates, aged 10–11 weeks at testing, as specified in **Supplementary Figure 2**. Electrophysiological recording and biocytin fillings were performed on the same KO and WT males that were tested in the Morris water maze and open field, with an >8 week interval after the last test, at the age of ∼16–20 weeks. For primary hippocampal cultures, E18 embryos were taken from pregnant WT (C57BL/6J) mice. All experiments were performed in accordance to Dutch law and licensing agreements and protocols were approved by the Animal Ethics Committee of the VU University Amsterdam.

## Behavioral Tests

Morris Water Maze (MWM), Passive Avoidance (PA), contextual Fear conditioning (cFC), and Open Field (OF) were carried out in four independent batches of animals (**Supplementary Figure 2**).

### Morris Water Maze (MWM) Test

Animals were handled for 1 week, two times a day, prior to MWM training. A circular pool (125 cm in diameter) was filled with opaque-colored (non-toxic dye) water and the water temperature was kept at 23–25°C. A round transparent escape platform (9 cm in diameter) was placed in the top left quadrant (target quadrant) of the pool, hidden 0.2 cm below the water surface. Geometric visual cues (1 m from the pool) were located on the walls of a dimly lit room (20 lx). Each mouse received a total of 2 daily swim sessions, each comprised of 2 swim trials (maximum duration 60 s per trial), with an interval of 2 min between sessions for 4 consecutive days. Before starting each training day, mice were placed on the platform for 30 s and then placed into the water at a semi-random start position (out of 4 start-positions). Mice that failed to find the platform were guided and placed on the platform for 15 s by the experimenter on day one. After each swim session, mice were returned to their home-cage for 2 min. Latency and distance swam to find the platform during training, and time spent and distance swam in the target quadrant in the probe test were examined using video tracking Viewer 2 (Biobserve, Bonn, Germany). Latency and distance to find the platform during training served as read-out of spatial memory acquisition. On the 5th day, the probe test (60 s) was performed, in which the platform was removed and mice were placed into the water opposite to the location of the platform/target quadrant. The time spent in each quadrant was recorded and time spent in the target quadrant served as measure of long-term spatial memory.

### Passive Avoidance Test

The pre-exposure, training, retention test, forced-exposure and 5-day extinction protocols were performed in a PA system (Model 256000, TSE-Systems, Bad Homburg, Germany). In the pre-exposure protocol, without unconditioned stimulus (US), mice were placed in the bright compartment (1000 lx) for 15 s. Then, a sliding door was opened for allowing the mice to explore the dark compartment (~10 lx) for a maximum period of 300 s. The training and retention test were performed as described before (Baarendse et al., 2008) with minor modifications in the US intensity (0.7 mA) and duration (2 s). The forced-exposure protocol was performed depending on the maximum time spent in the dark compartment during training, totaling 600 s. The extinction protocol was performed as the pre-exposure protocol, but now for a maximum period of 600 s. During the retrieval and extinction protocols, the latency to enter the dark compartment was measured as a read-out of long-term memory. Mice that did not enter the dark compartment during retrieval and extinction tests were recorded as a latency of 600 s. Boxes were cleaned with 70% ethanol between each experiment.

### Contextual Fear Conditioning

Contextual fear conditioning was carried out in a fear conditioning system (TSE-Systems, Bad Homburg, Germany) as described before (Schmitz et al., 2017). Long-term memory was assessed 24 h after training.

### Open Field

The open field test (OF) was performed in a white square box (50 × 50 cm, 35 cm high, 200 lx) by placing mice in the corner of the box and recording their exploration behavior for 10 min by video tracking (Viewer 2, Biobserve GmbH, Bonn, Germany). Time spent in the center area (32.9 × 32.9 cm) and total distance moved during the 10 min test were used as parameters for anxiety-like behavior and locomotor performance. Open field boxes were cleaned with 70% ethanol between each experiment.

## Primary Hippocampal Culture, Short Hairpin RNAs and Lentivirus Production

Hippocampal cultures were collected in Hanks balanced salts solution (HBSS; Sigma-Aldrich, St. Louis, MO, United States) with 7 mM HEPES (Life Technologies/Gibco, Carlsbad, CA, United States) and trypsin was added (10% final concentration; Life Technologies/Gibco) for 15–20 min at 37°C. Following two washing steps with HBSS-HEPES and one time with neurobasal medium [supplemented with 2% B-27, 1.8% HEPES, 0.25% glutamax and 0.1% penicillin/streptomycin (all from Life Technologies/Gibco)]. Cells were triturated with a fire-polished Pasteur pipette. After cell dissociation, neurons were plated at a density of $12.5 \times 10^3$ cells/well in a 96-well plate (Cellstar, Greiner Bio-One, Frickenhausen, Germany) coated with poly-D-lysine and laminin (Sigma-Aldrich) and treated with 5% heat-inactivated horse serum (Life Technologies/Gibco), or at a density of $75 \times 10^3$/well in a 12-well plate. Neurons were kept at 37°C/5% $CO_2$.

Short hairpin RNAs (shRNAs) were purchased from Sigma-Aldrich (Mission® shRNA bacterial glycerol stock; SHCLNG-XM_140850). Five shRNA were used to target and knockdown *Gpr158* gene expression and a scrambled shRNA (Sigma-Aldrich, pLKO.1-puro Non-Mammalian shRNA) was used as a control. Sequences for shRNA knockdown of the *Gpr158* gene were: shRNA#1 (TRC number: TRCN0000028697, sequence: CCGGGCCAAGTACATTTC GTTGTATCTCGAGATACAACGAAATGTACTTGGCTTTTT), shRNA#2 (TRC number: TRCN0000028716, sequence: CCGGGCTCATTATCACGGCTATATTCTCGAGAATATAGCC GTGATAATGAGCTTTTT), shRNA#3 (TRC number: TRCN0000028727, sequence: CCGGCCGGTCGTTATTCTG TACTTTCTCGAGAAAGTACAGAATAACGACCGGTTTTT), shRNA#4 (TRC number: TRCN0000028742, sequence: CCGGCGGCTATATTCCATACAATTACTCGAGTAATTGTAT GGAATATAGCCGTTTTT) and shRNA#5 (TRC number: TRCN0000028751, sequence: CCGGCCTTAACAACTCAGAG TGTATCTCGAGATACACTCTGAGTTGTTAAGGTTTTT).

Plasmids of shRNAs were plated on Lysogeny broth (LB) agar medium supplemented with ampicillin (Sigma). Single colonies were picked and grown in LB liquid medium supplemented with ampicillin using a shaker incubator at 37°C. DNA was extracted using NucleoBond Xtra Midi kit (Bioké, Leiden, Netherlands) according to the manufacturer's protocol. Lentivirus production were done using packaging, transducing and envelope constructs

at the same time for human embryonic kidney 293T cells transfection. Lentiviral particles were collected after 2 days of transfection and concentrated using ultracentrifugation (Beckman Coulter, Optima$^{TM}$ LE-80K).

Neurons were separately transduced with a *Gpr158*-targeting shRNA (see below) lentivirus at days *in vitro* 7 (DIV7). Briefly, neurons were transduced with 1:4000 titrated lentiviral particles in neurobasal medium supplemented with 2% B-27, 1.8% HEPES, 0.25% glutamax, 0.1% penicillin/streptomycin for each shRNA. Transduced neurons were kept at 37°C/5% $CO_2$. Cells for immunostaining were fixed at DIV14 using 4% PFA, 2% saccharose (VWR chemicals) in PBS (pH 7.4) for 20 min. Cells for quantitative real time PCR (qRT-PCR) experiments were harvested using Trizol reagent (Life Technologies) at DIV14.

## High-Content Screening for Neurite Morphology Analysis

Fixed neurons were washed with PBS and permeabilized with 0.5% Triton X-100 (Sigma-Aldrich) in PBS (Life Technologies) for 10 min. After washing, cells were blocked with 1% BSA (Sigma-Aldrich) and 0.1% Triton X-100 (Sigma-Aldrich) in PBS for 1 h. Neurons were stained with chicken anti-MAP2 (Bio-Connect, Huissen, Netherlands; 1:5,000) at 4°C overnight, and visualized using anti-chicken Alexa Fluor 647 (Life Technologies/Gibco; 1:400) for 90 min at RT. The nucleus was stained with Hoechst dye (1:10,000 in distilled water) for 10 min at RT.

Nuclei and neurites of neurons were imaged with Opera LX high-content screening system (PerkinElmer, Waltham, MA, United States). The 96-well plates were scanned with 10x magnification, sampling 40 images per well. All images were analyzed using Columbus software (PerkinElmer, v2.5.2). Briefly, neuron nuclei were dissociated from non-neuronal nuclei or debris based on morphological (nuclei area > 200 $\mu m^2$) and intensity (nuclei intensity > 100) parameters. Analyses were made at the population level of a well, taking the mean of selected neurons. Total neurite length (traced from the soma), number of protrusions (neurites branching) from the soma, number of first bifurcations (from soma protrusions), and number of extremities (neurite branching number from the first bifurcations) were calculated (see **Supplementary Figure 1**).

## Quantitative Real Time PCR for Gene Expression Analysis

Transduced neurons were collected with TRIZOL reagent (Life Technologies) at DIV14 and RNA isolation was performed accordingly using isopropanol (Sigma-Aldrich) precipitation (Spijker et al., 2004). RNA was quantified (NanoDrop ND-1000 spectrophotometer; NanoDrop Technologies, Wilmington, DE, United States). Random-primed (25 pmol; Eurofins MWG Operon; Ebersberg, Germany) cDNA synthesis was performed on individual RNA samples (100–125 ng total RNA) using MMLV reverse transcriptase (Promega). Real-time qPCR reactions (10 μL; Light cycler 480, Roche) and relative gene expression calculation were performed as described previously (Spijker et al., 2004; Schmitz et al., 2017). All qRT-PCR primers were designed

using Primer3.0 software and are listed (forward and reverse) as follows: *Gpr158*: 5'-AACACAGCCTAGATCCAGAAGAC-3' and 5'-GGGTTGTTTGTGATCATCTTTTTA-3'; *Gapdh*: 5'-TGCACCACCAACTGCTTAGC-3' and 5'-GGCATGGACT GTGGTCATGA-3'; β-*Actin*: 5'-GCTCCTCCTGAGCGCAAG-3' and 5'-CATCTGCTGGAAGGTGGACA-3'; *Hprt*: 5'-ATGGGA GGCCATCACATTGT-3' and 5'-ATGTAATCCAGCAGGTCA GCAA-3'.

## Slice Preparation, Electrophysiological Recordings and Morphological Reconstructions

Upon completion of the behavioral assessment, mice were swiftly decapitated and brains were extracted and placed for a short period, during transport to slicing room, in carbogenated (95% $O_2$, 5% $CO_2$) iced-cold 'slicing buffer' containing (in mM), 70 NaCl, 2.5 KCl, 1.25 $NaH_2PO_4.H_2O$, 5 $MgSO_4.7H_2O$, 1 $CaCl_2.2H_2O$, 70 Sucrose, 25 D-Glucose, 25 $NaHCO_3$, 1 Na-Ascorbate, 3 Na-Pyruvate; pH 7.4, 305 mOsm. Horizontal hippocampal slices (dorsal to ventral) were retrieved at 300 μm thickness, using a vibrating-blade microtome (HM-650V, Thermo Scientific), in ice-cold carbogenated 'slicing buffer,' where the dorsal to medial part of the hippocampus was taken. Each slice was briefly washed in 'holding ACSF' and placed in a slices chamber filled with carbogenated 'holding ACSF' containing in mM, 125 NaCl, 3 KCl, 1.25 $NaH_2PO_4.H_2O$, 2 $MgCl_2.6H_2O$, 1.3 $CaCl_2.2H_2O$, 25 D-Glucose, 25 $NaHCO_3$, 1 Na-Ascorbate, 3 Na-Pyruvate; pH 7.4, 305 mOsm. Slices were left to recover at RT for at least 1 h before recordings, and for the duration of the experimental day slices were maintained in the slice chamber containing 'holding ACSF.'

### Spontaneous Excitatory and Inhibitory Postsynaptic Current Recordings

Individual slices were transferred to a submerged recording chamber and left to equilibrate for 10 min, under continuous perfusion, at ~2 mL/min, with carbogenated 'recording ACSF' containing in mM, 125 NaCl, 3 KCl, 1.25 $NaH_2PO_4.H_2O$, 1 $MgCl_2.6H_2O$, 1.3 $CaCl_2.2H_2O$, 25 D-Glucose, 25 $NaHCO_3$; pH 7.4, 305 mOsm. Hippocampal CA1 pyramidal neurons were visualized under differential interference contrast microscopy, and selected based on their morphology. For sEPSC recordings in WT 10 cells from 4 animals, and in KO 14 cells from 4 animals were analyzed. For sIPSC recordings in WT 11 cells from 4 animals, and in KO 14 cells from 4 animals were analyzed. Whole-cell patch-clamp configuration was achieved using standard borosilicate glass pipettes, ~3–5 Mohm, filled with an Cesium-gluconate based intracellular containing in mM, 130 Cs-gluconate, 8 NaCl, 10 HEPES, 0.3 EGTA, 4 ATP-Mg, 10 $K_2$-Phosphocreatine, 0.3 GTP, 3 QX314-Cl, 0.3% Biocytin; pH 7.3, 290 mOsm. Recordings were conducted at ~32°C. Upon achieving a stable whole-cell configuration, up to 7 min of sEPSCs were recorded at a holding potential of −70 mV, and up to 7 min of sIPSCs were recorded at a holding potential of 0 mV (voltage clamp). The last 3 min of each trace were analyzed with mini Analysis software (Synaptosoft). Acquisition was performed

using p-Clamp software (Molecular Devices), using a Multiclamp 700B amplifier (Molecular Devices), sampled at 20 kHz, low-pass filtered at 6 kHz, and digitized with an Axon Digidata 1440A (Molecular Devices). Series resistance was monitored and only cells exhibiting less than 20% change were used for analysis. Cells whose access resistance exceeded 25 Mohm were also rejected.

### Paired Pulse Ratio Recordings

For PPR recordings of EPSCs, based on the observed change in decay time and similar to previously reported changes in PPR in the MF-CA3 pathway, whole-cell patch-clamp configuration was achieved with a κ-gluconate based intracellular containing in mM, 148 κ-gluconate, 1 KCl, 10 HEPES, 0.3 EGTA, 4 ATP-Mg, 4 $K_2$-Phosphocreatine, 0.4 GTP, 0.3% Biocytin; pH 7.3, 290 mOsm. For this experiment in WT 10 cells from 4 animals, and in KO 10 cells from 3 animals were analyzed. Upon achieving stable whole-cell configuration, action potential profiles (current clamp) were generated for each CA1 pyramidal, through current injections of 750 ms starting from −200 pA, at steps of 20 pA. These profiles were subsequently used to retrieve the passive and active properties form these cells. The resting membrane potential was measured during a 250 ms period prior to action potential profile generation. Subsequently, a unipolar stimulating electrode loaded with 'recording ACSF' was lowered near the location were Schaffer collaterals meet the patched-cell's dendrite. The electrode was moved around until a clear unisynaptic response could be observed, upon current injections mediated by a Master-9 pulse stimulator and an ISO-flex stimulus isolator (A.M.P.I). Thereafter, an input-output stimulation curve was generated by recording the patched cells' response to increasing amounts of current injections from 20 μA to 200 μA, at steps of 20 μA. For each step, 5 sweeps were averaged. The current intensity used during the PPR protocol was approximately the current generating half-maximal amplitude responses. The two pulses for the PPR protocol were separated by 50 ms, and 20–25 sweeps were recorded per cell. Data were analyzed with in-house Matlab (Mathworks) scripts. All other electrophysiological and technical parameters were as described in the section regarding sEPSC/sIPSC recordings.

### Biocytin Reconstructions

Upon completion of an electrophysiological recordings the pipette was slowly retracted to reseal the patched cell, and the slice was subsequently fixed in 4% paraformaldehyde (PFA), at 4°C for 48 h. PFA was replaced with PBS-Azide for long-term storage at 4°C until further analysis. The following set of cells was reconstructed. From the cells recorded under the PPR section, in WT 10 cells from 4 animals, and in KO 10 cells from 3 animals were analyzed. From the cells under the sEPSC/sIPSC section, in WT 8 cells form 3 animals (one animal is shared with the PPR experiment), and in KO 7 cells from 3 animals. For the per animal morphology, the aforementioned cells were averaged per animal, yielding in WT 18 cells from 6 animals, and in KO 17 cells from 6 animals. Slices containing biocytin filled cells, were incubated in 3% $H_2O_2$ in 0.05 M PB solution for 20 min, and then incubated for 48 h in 0.05 M PB containing 0.5% Triton X-100, and ABC complex solution (Vectastain; 1 drop solution A, 1 drop solution

B, per 20 mL volume). Subsequently, slices were incubated in 0.05 M PB containing 3.3 mM $H_2O_2$ and 2 mM diaminobenzidine tetrahydrochloride (DAB) under visual inspection. Incubation was terminated when a clear morphology could be visualized. All steps were separated by 3x washes in 0.05 M PB. Images of labeled cells were acquired with a light microscope (Olympus) at 20X magnification, using the Surveyor software (Objective Imaging). Reconstruction of the imaged cells was performed using the Neuromantic software (Myatt et al., 2012), and analysis of the reconstructed morphologies was performed using L-Measure (Scorcioni et al., 2008).

### Statistics

For genotype comparisons, two-tailed Student's *t*-tests (with or without correction for unequal variation) were applied for normally distributed data and Mann–Whitney *U*-tests otherwise. Normality was assessed with Kolmogorov–Smirnov and Saphiro–Wilk tests. In the case of normally distributed data but with unequal variances, Welch's unequal variance *t*-test was applied. Mixed ANOVA tests were carried out for genotype as between-subject factor and time as repeated measures (e.g., MWM training, PA extinction, I/O curve). A two-way ANOVA was applied to the morphological analyses at the animal level with genotype and type of dendrite as between-subject factors. All data pertaining to Principal component analysis (PCA) were generated using Matlab scripts (Mathworks). Multiple comparison correction for the correlation between cell surface and PCA variables was performed with the Bonferroni–Holm method. Three mice were removed from the MWM data set as they were floating instead of swimming [*Gpr158* KO $n = 1$ and WT $n = 1$, WT $n = 1$ (HZ batch)]. For electrophysiology, cells with values exceeding mean ± 2xSD were excluded (PPR/Properties: *Gpr158* KO $n = 1$, WT = 3; sEPSC/sIPSC: *Gpr158* KO $n = 4$, WT $n = 3$). Statistical significance level was set for *P*-values < 0.05. Statistical significance was assessed using SPSS v24 IBM, or Graphpad Prism 5 software (GraphPad Software, La Jolla, CA, United States) for Bonferroni *post hoc* tests.

## RESULTS

### *Gpr158* KO Mice Show Aberrant Spatial Learning and Decreased Acquisition of Safety Learning

Given the significant hippocampal expression of *Gpr158* (Allen brain atlas probe RP_051121_01_A10; Khrimian et al., 2017), not only in CA3 but also in the CA1 region (Ostrovskaya et al., 2018) (**Supplementary Figure 1**), we tested *Gpr158* KO mice and WT littermates in an array of hippocampal-dependent behavioral paradigms (**Supplementary Figure 2**). First, we performed MWM training with male Bl6/J *Gpr158* KO mice (**Figures 1A,B** and **Supplementary Figure 2**) and a probe test to assess long-term memory retainment of hidden platform location based on distal cues. During the 4-day training protocol, the distance swam to find the hidden platform was found statistically different in *Gpr158* KO mice *vs.* WT mice (**Figure 1A** and
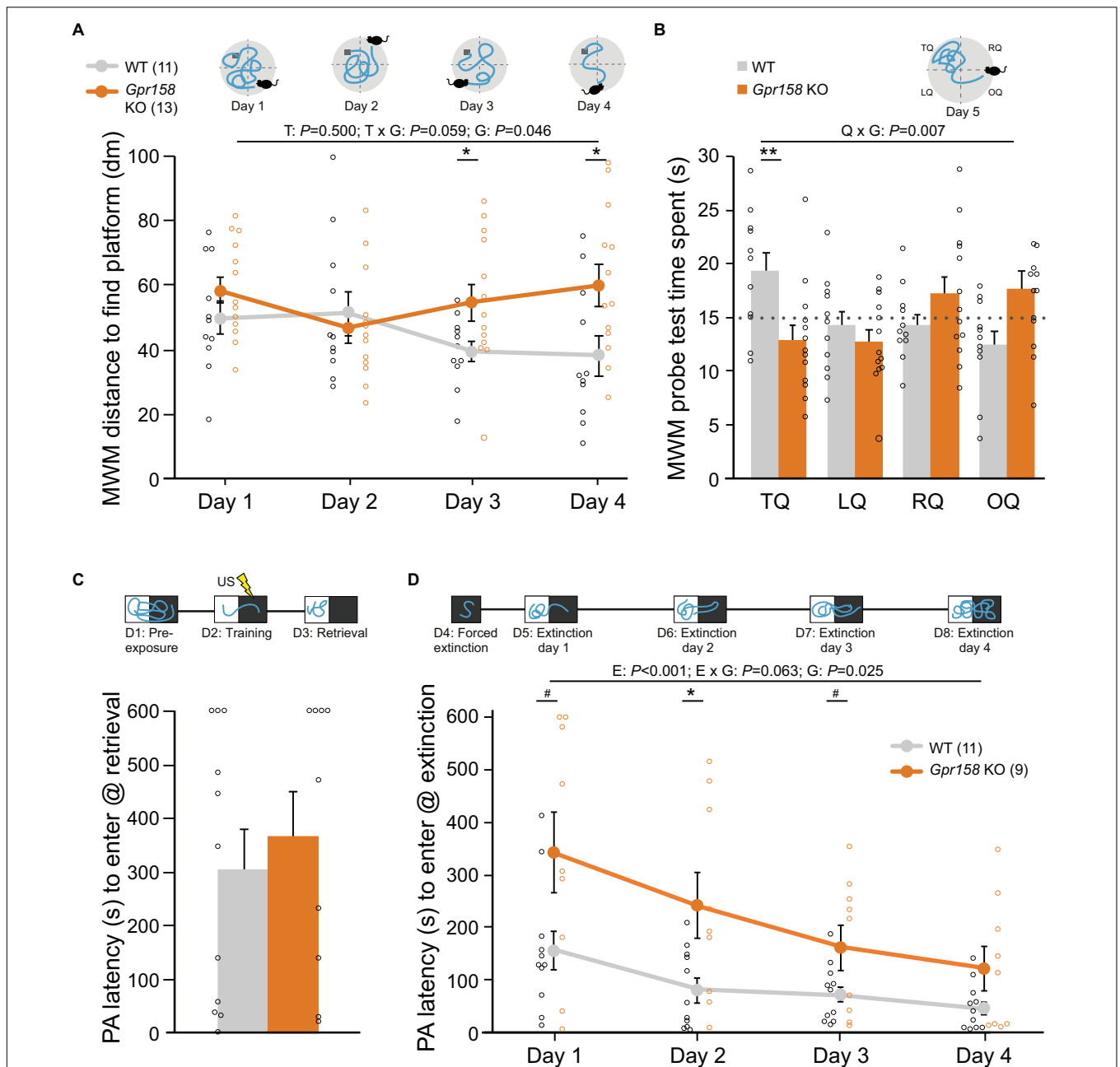
**FIGURE 1 |** *Gpr158* KO have a spatial memory deficit and show delayed safety learning. **(A,B)** Experimental set-up and data of training [see Online resource 3; **(A)** during four days of training, mice were placed in different locations in the circular pool and distance to reach the hidden platform (dark gray) was recorded], and probe test [**B**, time spent in each quadrant was recorded) in the Morris water maze (MWM). **(A)** During MWM training, *Gpr158* KO mice swam a longer distance to reach the platform and their performance did not reach WT levels [nWT = 11, nKO = 13; genotype (G) effect *P* < 0.046; training (T) effect *P* = 0.500, interaction *P* = 0.059]. **(B)** *Gpr158* KO mice showed a long-term memory deficit during the probe test [quadrant (Q) × genotype (G) *P* = 0.007], and spent less time in the target quadrant (TQ, RQ: right quadrant, LQ: left quadrant, OQ: opposite quadrant). **(C,D)** Experimental set-up and data of PA test and latency to enter the dark compartment after training **(C)** and during the four days after forced extinction **(D)**. **(C)** *Gpr158* KO mice (*n* = 9) showed similar PA retention as WT mice (*n* = 11). **(D)** After forced extinction in the dark compartment, *Gpr158* KO mice showed a delay in extinction learning [Extinction (E) *P* < 0.001, genotype (G) *P* = 0.025, interaction *P* = 0.063]. Data are presented as mean ± SEM with individual data points indicated. Asterisks and octothorpe indicate the level of significance between WT and KO assessed by Student's *t*-test/MWU test (**Supplementary Table 1**), #*P* ≤ 0.100; *P* ≤ 0.050; **P* ≤ 0.010.

**Supplementary Table 1**, mixed ANOVA: genotype *P* = 0.046; training *P* = 0.500, interaction *P* = 0.059), with *post hoc* testing showing increased distance in *Gpr158* KO mice *vs.* WT mice

during the last 2 training days (*t*-test: day 3 *P* = 0.031, day 4 *P* = 0.025). In addition, escape latency showed a similar effect (**Supplementary Figure 2** and **Supplementary Table 1**), albeit

the first training day showed an initial genotype difference in activity (**Supplementary Figure 2**). Whereas WT mice showed learning from day 1 to 4 (Latency: $P = 0.025$; Distance: $P = 0.012$), *Gpr158* KO mice did not (Latency: $P = 0.202$; Distance: $P = 0.831$).

Long-term memory was assessed with a 24 h retention interval after training during a probe session in which the platform was removed (**Supplementary Figure 2** and **Supplementary Table 1**). As the probe test measures the preferred location in a fixed time window it is able to dissociate memory from general activity, and as such it is relatively insensitive to altered swimming speed (Vorhees and Williams, 2006). *Gpr158* KO mice spent significantly less time in the target quadrant (TQ), indicative of long-term spatial memory impairments (**Figure 1B**, mixed ANOVA: interaction quadrant × genotype $P = 0.007$; $t$-test: TQ $P = 0.008$). The WT mice display a significant effect for quadrants ($P = 0.029$), but the KO mice did not ($P = 0.102$).

In addition, we tested *Gpr158* heterozygous (HZ) mice in the MWM test in order to see whether their spatial memory was affected as well (**Supplementary Figure 2** and **Supplementary Table 1**). MWM acquisition was not affected (mixed ANOVA: genotype $P = 0.312$; training $P < 0.01$, interaction $P = 0.320$), and both WT and HZ mice showed learning from day 1 to 4 (WT: $P < 0.001$; *Gpr158* HZ mice: $P = 0.029$). However, when tested in the MWM probe test, a deficit emerged (mixed ANOVA: interaction quadrant × genotype $P = 0.038$). Whereas the WT mice showed a good distinction between the former place of the escape location (quadrants $P = 0.038$), the HZ mice were unable to do so (quadrants $P = 0.539$), with a significant effect for the target quadrant (genotype $P = 0.042$). Overall, this indicated that the HZ *Gpr158* phenotype was milder than that of the full KO.

To distinguish between disturbed spatial processing deficits and motor or visual impairments possibly contributing to the observed changes, a visual platform test was performed 1 month after the probe test using a cue to signal the platform. Latency to find the platform was the same for *Gpr158* KO and WT mice during the visual platform trials (WT = 7.1 ± 1.1 s, *Gpr158* KO = 10.2 ± 2.0 s; $t$-test genotype $P = 0.201$, **Supplementary Table 7**). Additionally, when tested in the open field arena, anxiety-like behavior measured as distance moved and anxiolytic-like behavior measured as time spent in the center, was not different between genotypes (**Supplementary Figure 2**). Taken together, in the absence of motor and visual deficits or overt anxiety-like behavior, *Gpr158* KO mice exhibited spatial memory deficits in the MWM paradigm.

To assess context-specific memory, an independent batch of *Gpr158* KO and WT mice underwent a contextual fear conditioning (cFC) paradigm (**Supplementary Figure 2** and **Supplementary Table 1**). *Gpr158* KO mice did not have any fear memory deficit, exhibiting equal distance moved and freezing as WT during the retrieval test 24 h after conditioning; distance: $t$-test genotype $P = 0.715$; freezing: $t$-test genotype $P = 0.693$). To corroborate these results and to assess extinction of the acquired aversive memory we probed PA behavior, in an independent batch of mice, in which mice learn to avoid the preferred dark environment where a foot shock was delivered (**Figures 1C,D**). Long-term avoidance memory was tested on day 3, after pre-exposure (day 1) and training (day 2, **Figure 1C**). Both *Gpr158*

KO and WT mice showed the same level of retention (genotype MWU $P = 0.656$), corroborating the lack of contextual aversive memory deficits in *Gpr158* KO mice. Additionally, we assessed whether acquisition of extinction memory was different between genotypes (**Figure 1D**). To this end, we first performed a forced extinction session in the dark compartment in order to promote safety learning over response extinction only (Micale et al., 2017), and thereafter measured the latency to enter the dark compartment during the subsequent four days of extinction. This revealed a significant delay in extinction memory acquisition for *Gpr158* KO mice (**Figure 1D**, mixed ANOVA: Extinction $P < 0.001$, genotype $P = 0.025$, interaction $P = 0.063$; $t$-test genotype day 1 $P = 0.054$, day 2 $P = 0.020$; day 3 $P = 0.077$). Taken together, whereas *Gpr158* KO mice show no deficits in aversive memory acquisition, they do exhibit spatial memory deficits and difficulty in acquiring extinction memory, in the absence of motor and visual impairments or anxiety.

## Normal Basal Excitatory and Inhibitory Synaptic Transmission in *Gpr158* KO Mice

Abnormal synaptic transmission can alter information processing, affect learning and memory, and impact behavior (Mayford et al., 2012; Mitsushima et al., 2013). To that end, spontaneous excitatory and inhibitory post-synaptic currents (sEPSC and sIPSC) were recorded from CA1 pyramidal neurons from WT and *Gpr158* KO mice after completion of behavioral tasks (**Figures 2A–D** and **Supplementary Table 2**). Basal sEPSC frequency ($t$-test $P = 0.193$) and amplitude (MWU $P = 0.403$) was comparable between genotypes (**Figures 2A,B**). Although the decay time of sEPSCs was found prolonged in *Gpr158* KO cells ($t$-test $P = 0.047$; **Supplementary Table 2**), further analysis of the weighted tau of decay did not reveal any difference between genotypes (WT 9.79 ± 1.42 ms, KO 10.56 ± 1.91 ms, $t$-test $P = 0.294$, data not shown). Finally, rise time of sEPSCs was similar for both groups ($t$-test $P = 0.179$). Additionally, we did not observe any differences in the frequency ($t$-test $P = 0.470$) of sIPSCs (**Figures 2C,D**), however a trend for a reduction in amplitudes was identified (MWU $P = 0.058$). Inhibitory receptor kinetics were equal between genotypes ($t$-test, decay $P = 0.995$, rise $P = 0.314$). Taken together, our data from CA1 pyramidal neurons do not reveal any substantial difference in excitatory and inhibitory synaptic neurotransmission that could alter neuronal communication and impact behavior.

## Normal Release Probability but Reduced Schaffer Collateral-Mediated Responses in *Gpr158* KO Mice

A central feature in synaptic transmission is its ability to adapt to rapidly successive stimuli, which is regulated mainly by presynaptic mechanisms (Zucker and Regehr, 2002). The frequency of stimulation combined with synapse-specific release probabilities can filter activity, by allowing information transfer only when the appropriate conditions are met (Abbott et al., 1997; Fortune and Rose, 2001; Zucker and Regehr, 2002). To determine the excitability of CA3 to CA1 connections,
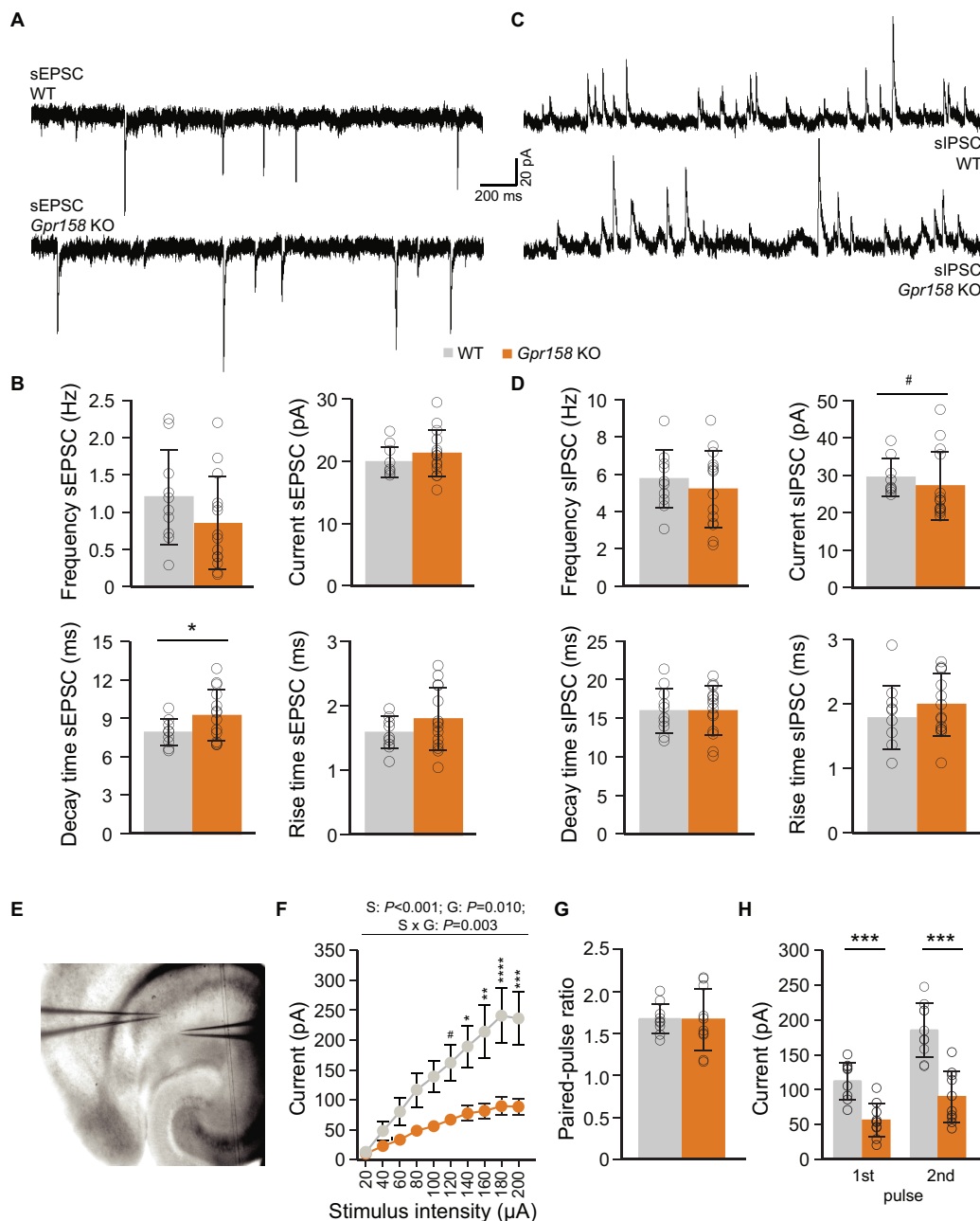
**FIGURE 2 |** Electrophysiological assessment of *Gpr158* KO CA1 pyramidal incoming synaptic transmission. **(A–D)** A cesium-gluconate-based intracellular was used to record both excitatory (**A,B**, WT *n* = 10 cells from 4 animals, KO *n* = 14 cells from 4 animals) and inhibitory (**C,D**, WT *n* = 11 cells from 4 animals, KO *n* = 14 cells from 4 animals) postsynaptic currents from CA1 pyramidal cells. Example traces of xcitatory **(A)** and inhibitory activity **(C)** recorded from WT and *Gpr158* KO mice. Frequency, amplitude, and rise time of sEPSCs were equal between genotypes **(B)**. A small increase in sEPSC decay time was observed in *Gpr158* KO (**Supplementary Table 2**). No difference was observed in sIPSC frequency, decay time, or rise time **(D)**. However, a trend for decreased sIPSC amplitude was observed in *Gpr158* KO (**Supplementary Table 2**). **(E–H)** For PPR recordings, a potassium-gluconate based intracellular was used for the recording pipette, while the stimulating pipette was loaded with aCSF and placed in a location where a clear unisynaptic response could be generated in the postsynaptic cell. Example configuration for I/O curve and PPR recordings (**E**; WT *n* = 10 cells from 4 animals, KO *n* = 10 cells from 3 animals). An I/O stimulation curve was generated by gradually increasing stimulation intensity in steps of 20 µA **(F)**. A clear reduction in postsynaptic responses was observed in *Gpr158* KO upon Schaffer collateral stimulation [stimulus (S): *P* < 0.001, genotype (G) *P* = 0.010; interaction *P* = 0.003] that became significant from 140 µA onward. A succession of two stimulations separated by 50 ms was applied at stimulation intensity approximately half-maximal to that generated during the I/O curve. The ratio between the 1st and 2nd response amplitude was equal between genotypes **(G)**. The raw amplitudes recorded during half-maximal stimulation during the PPR protocol differed significantly **(H)**. For panel **(F)** data are presented as mean ± SEM. For all other panels data are presented as mean ± SD with individual data points indicated. Asterisks and octothorpe indicate the level of significance between WT and KO assessed by Student's *t*-test or MWU (**Supplementary Table 2**), #*P* ≤ 0.100; *\*P* ≤ 0.050; \*\*\**P* ≤ 0.001.

an input-output (I/O) stimulation curve was generated, by stimulating Schaffer collaterals (SC) with increasing intensity, while recording from CA1 pyramidals (**Figure 2E**). *Gpr158* KO responses exhibited robust reduction for nearly all stimulation intensities, reaching plateau at below 100 pA, while WT responses plateau at just below 250 pA (**Figure 2F**, 2W-RMANOVA: genotype $P = 0.01$, stimulation $P < 0.001$, interaction $P = 0.003$; **Supplementary Table 2**). The reduction in responses was not due to differences in the placement of the stimulating electrode, since the distance between recording and stimulating electrodes was equal between groups (WT 77.51 ± 19.13 px, KO 86.39 ± 18.46 px, $P = 0.305$, data not shown). Subsequently, two successive stimuli were delivered, separated by 50 ms, at half-maximal stimulation intensities; current injected was not significantly different between genotypes (WT 90 ± 21.60 µA, KO 102 ± 12.76 µA, $P = 0.247$, data not shown). Surprisingly, the paired-pulse ratio (PPR), was equal between the two genotypes (**Figure 2G**, $t$-test $P = 0.945$), however, the raw amplitudes recorded during the PPR protocol where robustly different between WT and *Gpr158* KO mice (**Figure 2H**, $t$-test, 1st Pulse $P < 0.0001$, 2nd Pulse $P < 0.0001$). Therefore, our data suggest that even though presynaptic release probability and machinery could be intact, compromised SC integrity, synapse numbers, or vesicle load could drive the attenuated SC-CA1 responses.

### *Gpr158* Is Implicated in Hippocampal Neuronal Morphology

Dendritic architecture is central to the neuron's capacity to integrate signals, can influence cell intrinsic properties, and thus can impact learning and memory (Bekkers and Häusser, 2007). To that end, we investigated neuronal morphology both *in vitro* and *ex vivo* by analyzing WT hippocampal primary culture morphology after *Gpr158* knock-down (KD) (**Figure 3**), and by analyzing biocytin-loaded CA1 pyramidals in *Gpr158* KO and WT hippocampal slices (**Figure 4**). We used shRNA KD as approach because *in vitro* analysis of *Gpr158* KO primary neurons was hampered due to a severe reduction in viability (up to 95%).

Hippocampal primary neurons were initially transduced from day *in vitro* 1 (DIV1) until DIV14, with one of five different shRNA constructs (shRNA1-5) targeting different parts of *Gpr158* mRNA sequence, or a scrambled control shRNA (scRNA). This reduced cell viability to a similar extent as in *Gpr158* KO neurons. Hence, we transduced from day *in vitro* (DIV) 7 until DIV14 instead (**Figures 3A,B**). This window for transduction (DIV7–DIV14) seemed appropriate based on the *in vitro* developmental gene expression of *Gpr158* (**Supplementary Table 3**), and the efficiency of shRNA-mediated KD of *Gpr158* by DIV14 (**Supplementary Figure 3**). The KD effect as measured by gene expression was small, possibly due to an incomplete transduction, or by acting of these shRNAs on ribosomal entry of transcripts for translation, leaving mRNA largely intact. As such, the obtained data on the effect of the shRNA

KD might be underestimated, in the context of the large effects on morphology.

Different parameters were measured with respect to *in vitro* neuronal morphological development: total neuron number, total neurite length, number of protrusions from the soma, their bifurcations, and the number of extremities resulting from this (**Figure 3**, **Supplementary Figure 3**, and **Supplementary Table 3**). Although *Gpr158* KD reduced the survival of neurons for all shRNAs, shRNA4 and shRNA5 were the strongest affected, showing the largest response variability. For shRNA1-3 neuronal survival was compromised less, hence allowing for full morphological analyses (Online Resource 7, Kruskal–Wallis $P < 0.001$). All morphological parameters measured were affected by KD of *Gpr158* (**Figures 3C–E** and **Supplementary Figure 3**, Kruskal–Wallis, all $P < 0.001$). Specifically, neurite length was reduced by shRNA3 ($t$-test $P < 0.001$) and shRNA5 ($t$-test $P < 0.001$; **Supplementary Figure 3**). The number of bifurcations was reduced by shRNA2 ($t$-test, $P = 0.039$), shRNA3 ($t$-test, $P < 0.001$), and shRNA5 ($t$-test, $P < 0.001$; **Supplementary Figure 3**). Finally, the resulting number of extremities was reduced by shRNA3 ($t$-test, $P < 0.001$) and shRNA5 ($t$-test, $P < 0.001$; **Supplementary Figure 3**). Taken together, in the reduced conditions of primary culture, *Gpr158* KD disturbed development of neuronal morphology.

### Polarized Reductions in *Gpr158* KO CA1 Pyramidal Cell Dendritic Architecture

Given the impact that *Gpr158* KD had on neuronal morphology *in vitro*, we subsequently reconstructed the dendritic morphology from biocytin-loaded CA1 pyramidal neurons in hippocampal slices from adult *Gpr158* KO and WT mice (**Figure 4A**). In line with the observations *in vitro*, *Gpr158* KO CA1 pyramidals exhibited reduced total dendritic length (**Figure 4B**, $t$-test $P = 0.002$), as well as total surface area (**Figure 4B**, $t$-test $P = 0.002$; **Supplementary Table 4**). Moreover, the observed reductions in total length and surface area were supported by reductions specifically in the apical but not the basal dendritic compartment (**Figure 4B**, $t$-test: length [apical $P = 0.001$, basal $P = 0.346$], surface [apical $P = 0.002$, basal $P = 0.136$]). Furthermore, the general complexity of dendritic arborizations in *Gpr158* KO was reduced, reflected by the decrease in the total number of bifurcations per cell (**Figure 4B**, $t$-test: total $P = 0.002$, apical $P = 0.001$, MWU: basal $P = 0.481$). In contrast to the variable effect observed *in vitro*, the number of dendrites emerging from the cell body was equal (WT 7.40 ± 1.78, KO 7.70 ± 1.95, $t$-test $P = 0.723$, data not shown). The total number of branches was significantly reduced in *Gpr158* KO and the effect was specific to the apical dendritic compartment (**Figure 4B**, $t$-tests: total $P = 0.003$, apical $P = 0.001$; MWU: basal $P = 0.529$). Thus, the biocytin reconstructions of *Gpr158* KO CA1 pyramidal neurons *ex vivo*, illustrated reductions in dendritic architecture, paralleling *in vitro* observations, and localized the effect specifically to the apical dendritic compartment.

**FIGURE 3 |** *Gpr158* knock down leads to reduced neuronal outgrowth of hippocampal primary neurons. **(A)** Experimental set-up of *in vitro Gpr158* knockdown (KD). Viral transduction with independent shRNAs occurred from DIV7 to DIV14, and morphological analysis occurred at DIV14. **(B)** Representative images for control (scRNA) and *Gpr158* KD (shRNA1–5) neurons (red: MAP2, blue: nuclei). **(C–E)** Morphological analysis after *Gpr158* KD at DIV14 ($n$ = 7–8 wells; see Online Resource 6) shows an overall effect of the shRNA treatment for all parameters [neurite length **(C)**, number of bifurcations **(D)** and number of extremities **(E)**], as tested by Kruskal–Wallis ($P < 0.001$). Whereas shRNA3 affected all 4 parameters, the other shRNAs had a more limited effect for 1–3 of these parameters. Apart from a significant downregulation in number of protrusions, shRNA5 gave a similar strong effect as shRNA3, indicative of a *Gpr158*-related effect. Data are presented as mean ± SEM with individual data points indicated. Asterisks indicate significant differences compared with control (scRNA) assessed by Student's *t*-test (**Supplementary Table 3**), *$P \leq 0.050$; ***$P \leq 0.001$.

## Reduced Dendritic Architecture Correlates With Augmented Intrinsic Excitability of *Gpr158* KO CA1 Pyramidal Cells

Neuronal morphology contributes substantially to the integrative properties of neurons, and can have a major influence on neuronal firing by altering intrinsic cell properties (Bekkers and Häusser, 2007; Kowalski et al., 2016). Given the robust changes in neuronal architecture we documented both *in vitro* and *ex vivo*, we analyzed the action potential (AP) profiles from

WT and *Gpr158* KO CA1 pyramidal cells in hippocampal slices (**Figure 4C**) used for morphological assessment. For all positive current steps tested, the number of action potentials elicited was higher in the *Gpr158* KO CA1 pyramidals compared to their WT littermates (**Figure 4C**, 2W-RMANOVA: genotype $P = 0.010$, current injected $P < 0.0001$, interaction $P < 0.0001$; **Supplementary Table 4**). AP amplitude (**Figure 4D**, $P = 0.439$, **Supplementary Table 4**) and threshold (**Figure 4D**, $P = 0.311$) did not differ for genotype. However, both the minimum inter-spike interval (**Figure 4D**, ISI, $P = 0.015$) and minimum current required to elicit the first AP (**Figure 4D**, rheobase, $P = 0.009$)
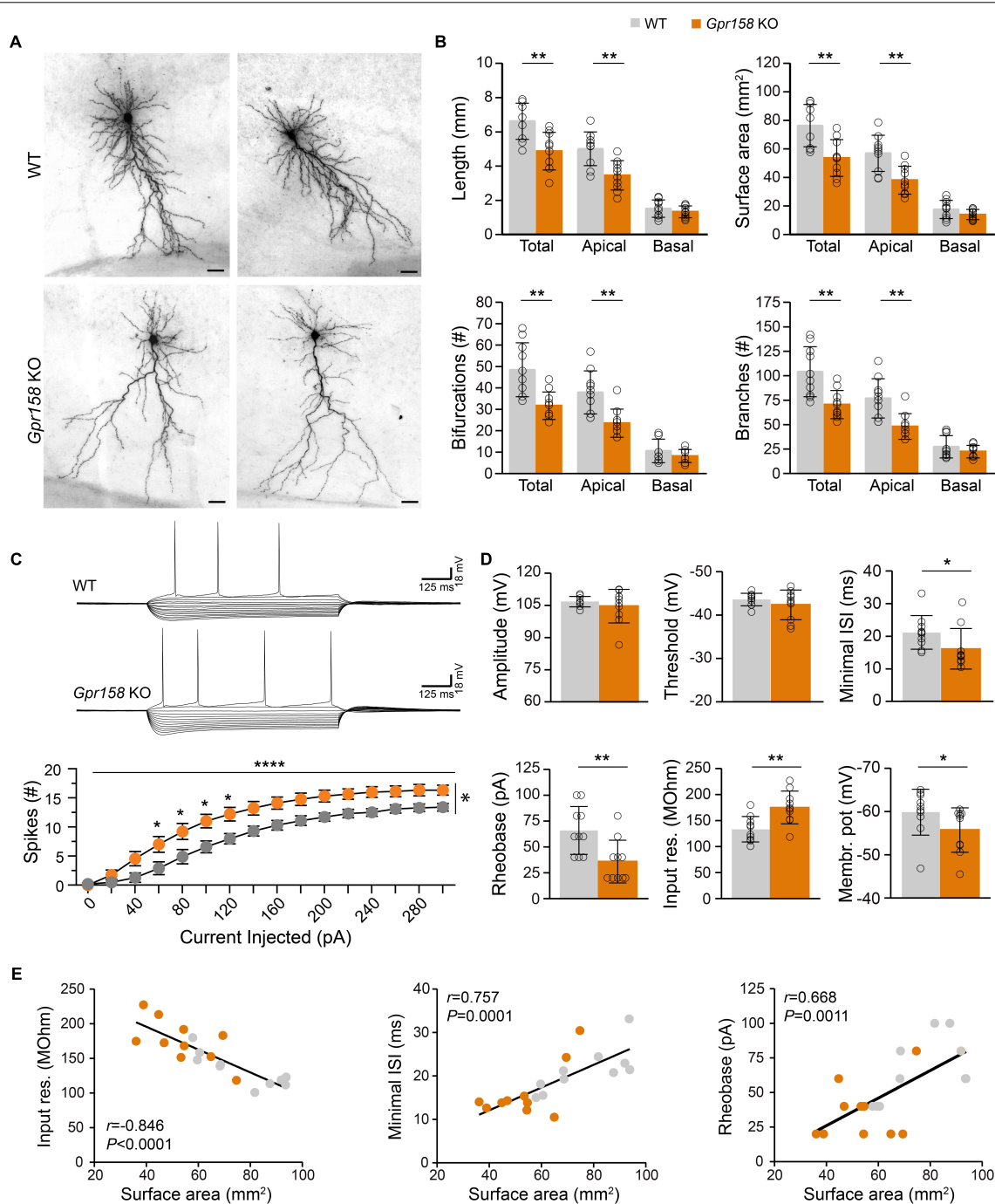
FIGURE 4 | Reduced dendritic architecture supports hyperexcitability of *Gpr158* KO CA1 pyramidal neurons. (A) Examples of CA1 pyramidal cells loaded with biocytin during electrophysiological recordings from WT (n = 10 cells from 4 animals) and *Gpr158* KO (n = 10 cells from 3 animals) hippocampal slices. Cells were subsequently reconstructed and their basic morphological measures were extracted and analyzed (Online Resource 8). (B) Total dendritic length and surface area were significantly reduced in *Gpr158* KO CA1 pyramidals and the effect was specific to the apical compartment. A significant reduction in total and apical but not basal compartments was documented for the number of bifurcations and number of branches. (C,D) For each reconstructed cell, the full action potential profile was generated and analyzed. (C) Example traces of WT and *Gpr158* KO action potential profiles generated by current injections in steps of 20 pA. Note that increased number of spikes were observed for all current steps tested in the *Gpr158* KO. (D) Action potential amplitude and threshold was unaffected by genotype. Minimum inter spike interval and rheobase were significantly reduced in *Gpr158* KO pyramidal cells. In addition, input resistance was increased in *Gpr158* KO and the membrane potential was more depolarized in *Gpr158* KO pyramidal cells. (E) Significant Pearson correlations (r) and linear regression (**Supplementary Figure 4**) between cell surface area and input resistance (r = −0.846, P < 0.0001), minimum inter spike interval (r = 0.757, P = 0.0001), and rheobase (r = 0.668, P = 0.0011). Data are presented as mean ± SD; individual data points are indicated. Asterisks indicate significant differences compared with WT cells assessed by Student's t-test or MWU (**Supplementary Tables 4, 5**), *P ≤ 0.050; **P ≤ 0.010; ****P < 0.001.

were reduced, underlying increased excitability of *Gpr158* KO pyramidals. Moreover, the input resistance (Ri) of *Gpr158* KO cells was significantly increased, further substantiating and promoting their increased excitability (**Figure 4D**, $P = 0.004$). Neuronal cell membrane time constant did not differ between the two groups (WT: $29.92 \pm 4.84$ ms, KO: $27.77 \pm 4.42$ ms, $P = 0.312$, data not shown). Finally, the resting membrane potential of *Gpr158* KOs was found more depolarized than in WT (**Figure 4D**, $P = 0.035$). Notably, ISI was also significantly reduced when cells were clamped at $-70$ mV (WT: 24.8 ms, KO: 16.5 ms; $P = 0.001$) and rheobase was reduced as a strong trend (WT: 90 pA, KO: 75 pA; $P = 0.055$) (**Supplementary Figure 4** and **Supplementary Table 4**), excluding confounding effects that our reported difference in resting membrane potential could cause.

We then applied PCA on the morphological and electrophysiological parameters collected from the same cells to dissect the most significant determinant underlying the changes observed (**Supplementary Figure 5**). For all components, cell surface area was the variable with the most significant contribution (**Supplementary Figure 5**, first 3 components shown). A subsequent correlation matrix of surface area against all other morphological and electrophysiological variables demonstrated significant correlations with all morphological measures, with cell excitability, and with PPR raw amplitudes (**Supplementary Figure 5**). However, upon multiple comparison correction, the correlation between surface area and raw PPR amplitudes did not retain significance, while the rest retained high statistical significance (**Supplementary Figure 5**). Subsequent linear regression demonstrated that surface area negatively correlated with Ri (**Figure 4E**, $r = -0.846$, $P < 0.0001$), whereas a positive relationship was demonstrated with minimum ISI (**Figure 4E**, $r = 0.757$, $P < 0.001$), and rheobase (**Figure 4E**, $r = 0.668$, $P = 0.001$). Taken together, our data demonstrated that *Gpr158* KO CA1 pyramidal cells exhibit increased excitability, and that this increase might be driven by their notable reduction in dendritic architecture.

## Reduced Architecture of CA1 Pyramidal Neurons Correlates With MWM Learning Deficits

Changes in the excitability of neurons can alter information flow, whereas changes in dendritic architecture can also impact the integrative capacity of neurons (Magee, 2000; Bekkers and Häusser, 2007; van Elburg and van Ooyen, 2010). Moreover, dendritic complexity appears to increase with evolution and with increasing cognitive demands, with human prefrontal pyramidals exhibiting the largest cortical dendritic complexity (Elston et al., 2001; Mohan et al., 2015). Furthermore, increasing dendritic complexity of human cortical pyramidals appears correlated with increasing intelligence quotient, in a small sample of surgically resected brain tissue (Goriounova et al., 2018). Since the electrophysiological datasets reported here were generated from mice that underwent behavioral assessment (**Supplementary Figure 2**), we then averaged the morphology data of all cells collected to generate an overview of dendritic architectures for $n = 6$ animals per genotype (**Figure 5A**).

Analysis of the combined morphologies further substantiated the robust reduction in dendritic architecture of *Gpr158* KO hippocampal neurons [**Figure 5A**, 2W-ANOVA, genotype (G) effect; length $P = 0.002$; surface $P < 0.001$; bifurcations $P < 0.001$; branches $P = 0.001$; **Supplementary Table 5**]. Furthermore, the effect was specific to the apical but not the basal dendritic compartment [**Figure 5A**, 2W-ANOVA, dendritic compartment (DC) effect; for all measures $P < 0.001$]. Apical ($P < 0.001$) but not basal dendritic length (all $P > 0.300$) was reduced in *Gpr158* KO mice, as well as surface area, number of branches, and number of dendritic bifurcations in the same manner (**Supplementary Table 5**).

Given the emergence of surface area as major determinant for the morphological and electrophysiological differences observed, we further probed its relationship with MWM parameters for the entire group of mice. For the MWM probe test, neither the distance covered in the TQ (**Figure 5B**, Spearman $r = 0.538$, $P = 0.071$), nor the time spent in the TQ (**Figure 5B**, Spearman $r = 0.322$, $P = 0.308$) were significantly correlated with the animal's apical dendritic surface area. However, for the acquisition of the MWM task, surface area did significantly and negatively correlate with both the distance covered to reach the platform (**Figure 5C**, Spearman $r = -0.643$, $P = 0.024$), and with the latency to reach the platform (**Figure 5C**, Spearman $r = -0.680$, $P = 0.015$). Therefore, the reduction in general dendritic architecture in *Gpr158* KO CA1 neurons, although not directly affecting long-term MWM memory, demonstrated a significant and negative correlation with the acquisition of this spatial memory task.

## DISCUSSION

In this study we report that mice deficient of *Gpr158* exhibit impairments in the acquisition and retrieval of spatial memory in the MWM paradigm, as well as deficits in the learning of an extinction memory in the PA task. Although hippocampal CA1 basal excitatory and inhibitory neurotransmission was found normal, we report a remarkable reduction in the excitability of SC synapses onto CA1 pyramidals, whereas we observed a potential compensatory increase in the intrinsic excitability of these neurons. Strikingly, both *in vitro* and *ex vivo* we observe a large effect of reduced *Gpr158* levels on dendritic morphology. *Ex vivo*, the dendritic architecture reductions of CA1 neurons was specific for the apical but not the basal compartment of these cells. Finally, the reduced apical complexity of these neurons appears to support the spatial memory acquisition deficits in these mice, since reduced neuronal surface area positively correlated with poor performance during acquisition of the MWM task.

### Behavioral Analysis

For *Gpr158* KO, a robust anxiety phenotype was detected previously (Khrimian et al., 2017). Here, we do not report such anxiety-like phenotype, neither in a novel open field, nor when placed in the fear conditioning box prior to conditioning. This might relate to the fact that the genetic background of mice of the Knockout Mouse Project (KOMP) repository is C57BL/6NTac
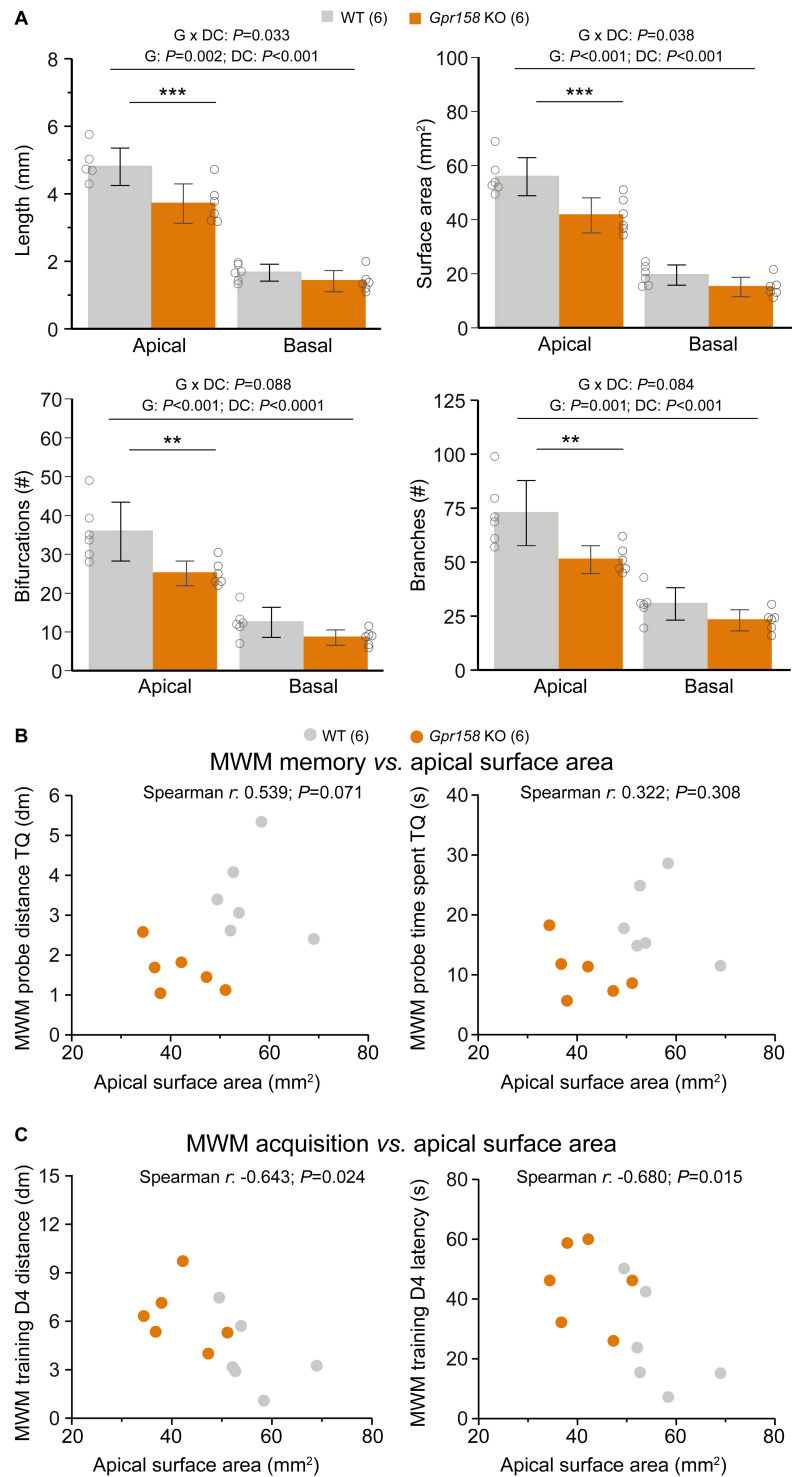
**FIGURE 5 |** Reduced dendritic architecture negatively impacts learning during MWM training. **(A)** Cell morphology from all the electrophysiological data sets described were averaged to generate an overview of hippocampal dendritic architecture per animal (WT $n$ = 6 animals, 18 cells averaged, KO $n$ = 6 animals, 17 cells averaged). Apical but not basal hippocampal dendritic length, surface area, bifurcations and branches were significantly reduced in *Gpr158* KO animals. **(B)** Apical surface area did not (significantly) correlate with either the distance covered ($P$ = 0.071) or the time spent ($P$ = 0.308) in the target quadrant (TQ) during the MWM probe test assessing long-term memory. **(C)** During acquisition of the MWM task, the apical surface area did significantly and negatively correlate with both the distance covered to reach the platform ($P$ = 0.024) and the latency ($P$ = 0.015) reaching the platform on the last training day (D4). Data are presented as mean ± SD with individual data points indicated. Asterisks indicate significant differences between WT and KO assessed by Student's $t$-test (**Supplementary Table 5**), **$P$ ≤ 0.010; ***$P$ ≤ 0.001.

whereas Khrimian et al. (2017) kept their mice on a mixed 129-Sv/C57BL/6J background. The 129-Sv background is known for its anxiety (Tarantino et al., 2000; Rodgers et al., 2002), even when used in a mixed background (Võikar et al., 2001), and anxiety can be a confounding factor in cognitive performance (Brooks et al., 2005).

Neither did we find an anxiolytic phenotype as previously measured in the EPM, TST and FST (Sutton et al., 2018) using the same KO line and strain, when considering the classical open field test, or when analyzing locomotor data from other tests. Given the observed genotype effect only in acquisition of safety memory, but not in initial acquisition of the avoidance memory in the same task, our read-out on cognitive function is unrelated to the emotional impact of the test. As such, the lack of a baseline anxiolytic phenotype allows for explicit interpretation of the different contextual fear paradigms. Initial fear acquisition and acquisition of safety memory (see below) likely represent different forms of learning, in which the first is apparently not dependent on the Gpr158 circuitry, but the latter, as well as acquisition and recall of spatial memory is.

## Acquisition of a Safety Memory and Spatial Memory Are Affected in *Gpr158* KO Mice

Non-spatial memory acquisition and expression, as measured in the PA test, and in contextual fear conditioning with context as the foreground stimulus, was not affected in *Gpr158* KO mice. However, normalization of avoidance behavior after forced exposure to the conditioning context was delayed in *Gpr158* KO mice. This safety learning procedure has been shown to rely on hippocampus CB1 receptors (Micale et al., 2017), in contrast to response extinction learning, i.e., repeated execution of the avoided response in absence of negative consequences, that is largely cortically mediated. Single intrahippocampal injection of cannabinoid-related compounds prior to safety learning acquisition could alter the effect of safety learning (Micale et al., 2017). Additionally, these compounds affected the propagation of signaling from the DG via area CA3 to the CA1 subfield upon perforant pathway stimulation (Micale et al., 2017). Thus, the reduced SC-mediated responses we observed in hippocampal slices of *Gpr158* KO mice might indicate that information processing within the trisynaptic circuitry of the hippocampus is disturbed. As such this precipitates not only in impaired safety learning, but also in poor spatial memory acquisition and expression, which is also dependent on balanced cannabinoid signaling in the hippocampus (Abush and Akirav, 2010).

During training in the MWM paradigm, *Gpr158* KO mice exhibited robust deficits in task acquisition, demonstrated by their increased distance covered and time spent to reach the platform. This is in line with a previous observation of impaired MWM acquisition in these mice (Khrimian et al., 2017). We additionally report that *Gpr158* KO mice demonstrated a long-term spatial memory deficit, highlighted by the reduced performance during the MWM probe trial. During the probe test, the platform is removed and the animal is requested to rely on spatial information to relocate the area of the previous escape platform after a 24 h interval. The hippocampus plays a major role in spatial learning, with involvement of both the CA1 and CA3 regions (Florian and Roullet, 2004), in which *Gpr158* is expressed (Khrimian et al., 2017; Condomitti et al., 2018). Theta frequency coupling between CA3 and CA1 is enhanced during MWM learning, when there is a clear improvement in task performance (Hernández-Pérez et al., 2016). The changes in CA1 morphology and excitability we report along with the changes in CA3 physiology (Condomitti et al., 2018) could alter such coupling, hence impacting learning in *Gpr158* KO mice. Although the CA3 region is involved in spatial memory acquisition, it is not required for long-term memory recall during the probe test (Florian and Roullet, 2004) that we here report as also being affected in *Gpr158* KO mice. Enhanced CA1 LTP, is shown to improve MWM probe test performance (Okada et al., 2003). Although not yet demonstrated to be different in the CA1 in *Gpr158* KO mice, LTP deficits in the CA1 region akin to those described in CA3 (Condomitti et al., 2018) are likely – as discussed below, and could support deficits in spatial memory acquisition.

## Reduced Dendritic Architecture Supports Spatial Memory Learning Deficits

Changes in spine density and size have been previously demonstrated in *Gpr158* KO mice in the CA3 area of the hippocampus (Condomitti et al., 2018), in a pathway-specific manner. Despite the increase in spine density, there was mostly an increase in thin spines, and at the ultrastructural level, synapses showed reduced active zone and PSD length. This suggests that at least in the MF-CA3 pathway *Gpr158* KO mice show an immature morphological phenotype, similar to our *in vitro* data. Whether similar changes in dendrite length occur in the CA3 as they do in the CA1 remains to be determined.

Central to our observations are the striking reductions in dendritic architecture and complexity of *Gpr158* deficient neurons *in vitro* as well as *ex vivo* in the CA1 region. Albeit that the effects *in vitro* in hippocampal cultures was variable across the 5 different shRNAs used, which may include possible off-target effects, this morphological phenotype was largely replicated *ex vivo* in reconstructed CA1 pyramidals within hippocampal slices. Complex dendritic architecture is essential to proper learning and memory (Elston et al., 2001). Dendritic complexity increases with evolution and with increasing cognitive demands (Tronel et al., 2010), and impairments in dendritic architecture have been observed in disorders with reduced cognitive capacities (Kulkarni and Firestein, 2012). Moreover, dendritic structure impacts the integrative ability of neurons, through pathway-specific distinct input domains, coincidence detection, synaptic scaling of distal inputs, and targeted dendritic inhibition, to name a few (Spruston, 2008).

Importantly, the reduced architecture we observed, negatively correlated with the last days of spatial memory acquisition in the MWM paradigm but not significantly with probe test performance. Spatial learning itself has been shown to enhance dendritic complexity by increasing length, bifurcations, and

branches of DG new born granule cells, in rats trained in MWM and in the delayed matching-to-place task (Tronel et al., 2010). Mostly these learning-induced changes are relatively small and short-lasting. Instead, genetic-induced mutations that affect dendritic architecture during development could have a higher impact. Hence mutation-associated learning deficits could arise through changing specific plasticity mechanisms. Mutant mice for tyrosine kinase *Fyn*, involved in normal cell physiology, exhibit deficits in MWM acquisition and recall, along with impairments in CA1 LTP, and reduced compaction and organization of CA1 apical dendrites (Grant et al., 1992). In addition, mice double mutant for cysteine proteases calpain 1 and 2 exhibit impaired spatial memory in MWM, in the absence of visual or motor deficits or anxiety-like behavior in the open field (Amini et al., 2013). Electrophysiological analysis revealed that CA1 pyramidal dendritic complexity, LTP, and CA3 to CA1 I/O curve were robustly reduced in these mutants (Amini et al., 2013). It is therefore likely that the reduced dendritic architecture of *Gpr158* KO CA1 pyramidals we report here could faithfully underlie the deficits in spatial memory acquisition, potentially through impairments in the amplitude and temporal course of EPSPs and induction and expression of LTP.

In the SC to CA1 network, brain-derived neurotrophic factor (BDNF) is required for the induction and maintenance of LTP brought about by repeated dopamine stimulation in apical but not in basal dendrites (Navakkode et al., 2012), and hippocampal BDNF levels in *Gpr158* KO are found reduced (Khrimian et al., 2017). To date, impaired PPR and LTP in *Gpr158* KOs has been reported for the MF to CA3 pathway (Khrimian et al., 2017; Condomitti et al., 2018), but LTP has not been investigated for the CA3 to CA1 pathway. Although we report normal PPR for this pathway, given the robust reduction in CA3 to CA1 stimulation and deficient dendritic architecture we observe, along with reduced hippocampal BDNF levels (Khrimian et al., 2017), CA3 to CA1 LTP could be impaired in *Gpr158* KO as well, and as such be driving impairments in spatial memory.

## Normal Basal Synaptic Transmission and Increased Excitability of *Gpr158* KO CA1 Pyramidals

Along with the changes in dendritic architecture, we observed an overall increase in the excitability of the reconstructed cells. *Gpr158* KO pyramidals elicited more action potentials than WT pyramidals for all positive current steps. Furthermore, rheobase as well as minimal ISI were significantly reduced in *Gpr158* KO CA1 pyramidals, independent of the resting membrane potential, whereas input resistance was increased and resting membrane potential was more depolarized. Moreover, PCA revealed that these changes were strongly correlated with the cell surface area. The contribution of the dendritic tree to neuronal excitability has been elegantly demonstrated, whereby pinching or severing neuronal dendrites significantly increased action potential frequency and input resistance, while reducing rheobase (Bekkers and Häusser, 2007). As such, our observations of increased CA1 pyramidal excitability in *Gpr158* KOs could be governed by their reduced dendritic morphology.

The increased excitability observed in *Gpr158* KO could possibly compensate for the reduced SC drive, as previously reported in an epilepsy model (Dinocourt et al., 2011). A hallmark of CA1 neurons is the ability to show action potential backpropagation, which is important for the integration of synaptic input and the induction of synaptic plasticity. Dendritic architecture, and specifically the number of dendritic branchpoints, showed a strong relationship with the functional threshold of backpropagation (Vetter et al., 2001), with lower number of branchpoints having a lower requirement of Na-channels to induce backpropagation as shown by computational modeling. As such, a lower threshold to induce backpropagation could compensate for the reduced SC drive. The reduced SC drive, as measured by the lowered I/O response, in *Gpr158* KO animals could relate to putative changes in the total number and/or the density of excitatory synapses (akin to that observed in CA3, see above), although this conclusion is not supported by a change in the sEPSC frequency. Alternatively, changes in passive and active properties of CA1 PC dendrites might play a role. Taken together, these morphological changes could contribute to the integrative capacity of CA1 pyramidal neurons.

Basal synaptic transmission onto CA1 pyramidal cells appears unaffected in *Gpr158* KO hippocampus, with no notable changes in either spontaneous excitatory or inhibitory frequency and amplitude observed. This is in contrast the reductions observed in sEPSC frequency and amplitude in *Gpr158* KO CA3 (Condomitti et al., 2018). Along with the reductions in evoked AMPA and NMDA CA3 currents (Condomitti et al., 2018) as well as the reduced SC mediated responses we observe, it is conceivable that when the network is further challenged, or when miniature release is assessed, such changes may become apparent in CA1 as well. Albeit, reduced CA3 to CA1 input does not always impact basal synaptic transmission (Grant et al., 1992; Amini et al., 2013). In the mPFC L2/3, increased spontaneous excitatory frequency (Sutton et al., 2018) is observed alongside increased excitability (Song:2019ft). In particular the latter phenotype, which is linked via cAMP-dependent phosphorylation to the A-type potassium channels shows layer-specificity, highlighting the possibility of brain area and pathway-specific alternations caused by *Gpr158* deficiency.

## Is *Gpr158* an Inducer of Presynaptic Organization in CA1 Akin to Its Role in CA3?

A major contributing factor in affecting *Gpr158* KO CA1 pyramidal morphology is incoming presynaptic activity. In the rodent hippocampus, mechanical perforant pathway denervation leads to sustained reductions in dendritic length and complexity of the postsynaptic dentate gyrus granule cells (Vuksic et al., 2011). Importantly, these reductions were observed primarily in the outer molecular layer where denervation had occurred. Additionally, deafness or facial nerve lesions resulted in pathway-specific reductions in dendritic morphology, in either primary auditory cortex (Bose et al., 2010), or primary motor cortex pyramidal cells (Urrego et al., 2015), respectively. The attenuated responses of SC stimulation we report, along with the reported

reduction in CA3 pyramidal excitability (Condomitti et al., 2018), could lead to reduced SC output. Yet, our reconstruction of *Gpr158* KO CA1 pyramidals revealed that structural reductions were specific to the apical but not basal dendritic compartments. Consequently, attenuated excitation of CA1 apical dendrites by SC might promote the compartment-specific morphological alternations we report here. However, whether this stems from pathway-specificity and how such specificity is obtained is not clear, as CA3 SC project both to apical and basal dendrites. Albeit, Gpr158 could be required for the formation of SC to apical but not basal CA1 dendritic synapses.

In the MF-CA3 pathway, Gpr158 functions as a post-synaptic organizer (Condomitti et al., 2018), where it has a specific role in shaping synapse morphology and function in apical dendrites within the MF-CA3 pathway, but not within the CA3-CA3 recurrent pathway. This is largely ascribed to the enriched subcellular localization of Gpr158 to apical dendrites in the stratum lucidum (Condomitti et al., 2018). With the specific effect in the apical part of CA1 dendrites in *Gpr158* KO mice, one could assume that subcellular localization of Gpr158 in CA1 neurons is similar to that of CA3 neurons. As such, it raises the possibility that the CA1 dendritic phenotype is independent of SC input and instead that SC input is induced by malformed synaptic contacts due to a lack of normally enriched levels of Gpr158. Nonetheless, future experiments using conditional KO mice can be aimed to precisely dissect the pre- vs. postsynaptic role of Gpr158 in CA1 circuitry in more detail. Our *in vitro* KD data also suggest a morphological role during development of Gpr158. Transduction of *Gpr158* shRNAs at hippocampal primary neurons at DIV7 showed at least in two out of five a major effect on dendritic outgrowth and maintenance in the weeks thereafter. Taken together, lack of the post-synaptic organizer *Gpr158* itself, and/or the resulting altered dendritic morphology, could subsequently shape presynaptic SC input.

Recently, to the growing set of post-synaptic organizers of the hippocampus CA1 (Thakar et al., 2017) another three important factors have been added recently (Schroeder et al., 2018), i.c. Flrt2, Lrrtm1, and Slitrk1. The authors elegantly showed that these factors affect synaptic organization in a different manner, and that they are expressed in overlapping sets of neurons, with a ~23% probability of being expressed all together at the same synapse with PSD-95. *Gpr158* expression in CA1 has a temporal shift compared with that in CA3. Knowing that synapse formation starts at PD7 and continues until PD28, and that *Gpr158* expression in CA1 starts at PD10-14 and reaches adult-like levels in term of CA1/CA3 ratio at PD28 (Khrimian et al., 2017; Condomitti et al., 2018), Gpr158 could well function together with the growing set of CA1 postsynaptic organizers in a subset of SC-CA1 connections. An outstanding question remains which CA3 expressed presynaptic organizer interacts with postsynaptic Gpr158 to form CA3-CA1 synapses. From the recently reported 129 interactors (Orlandi et al., 2018), 12 were extracellular matrix-related, and of these several are expressed at low-high levels in CA3 (**Supplementary Table 6**).

Taken together, we here showed that apart from the previously reported important role of Gpr158 in the MF-CA3 pathway, also the CA3-CA1 pathway is affected by loss of *Gpr158*.

Specifically, we showed that CA1 dendritic morphology and synaptic function is related to the spatial learning deficit that *Gpr158* KO mice display.

## DATA AVAILABILITY STATEMENT

All datasets generated for this study are included in the article/**Supplementary Material**.

## ETHICS STATEMENT

All animal experiments were performed in accordance with Dutch law. The licensing agreements and protocols were reviewed and approved by the Animal Ethics Committee of the VU University Amsterdam.

## AUTHOR CONTRIBUTIONS

DÇ, RL, and SS performed the behavioral experiments. DÇ analyzed the results. TG made the hippocampal cultures. DÇ performed and analyzed the *in vitro* studies and was supervised by TG and SS. YG produced and tested the virus. IK performed and analyzed the electrophysiological studies as well as the morphological reconstructions. IK, DÇ, AS, KL, and SS participated in the design of the study. SS, AS, KL, and HM supervised the project. IK and SS performed full statistical analyses of the data (electrophysiology/morphology and behavior/*in vitro* culture, respectively) and wrote the manuscript. All authors read, helped to revise and approved the final version of the manuscript. SS confirms to have seen and approved the raw data of all experiments (**Supplementary Table 7**).

## FUNDING

## ACKNOWLEDGMENTS

for their technical assistance. Additionally, we would like to thank Dr. Christian de Kock for access to the morphology acquisition recourses and Dr. Oliver Stiedl for setting up the passive avoidance test. This manuscript has been released as a preprint at bioRxiv (Çetereisi et al., 2018).

# SUPPLEMENTARY MATERIAL

# REFERENCES

Abbott, L. F., Varela, J. A., Sen, K., and Nelson, S. B. (1997). Synaptic depression and cortical gain control. *Science* 275, 220–224.

Abush, H., and Akirav, I. (2010). Cannabinoids modulate hippocampal memory and plasticity. *Hippocampus* 20, 1126–1138. doi: 10.1002/hipo.20711

Amini, M., Ma, C.-L., Farazifard, R., Zhu, G., Zhang, Y., Vanderluit, J., et al. (2013). Conditional disruption of calpain in the CNS alters dendrite morphology, impairs LTP, and promotes neuronal survival following injury. *J. Neurosci.* 33, 5773–5784. doi: 10.1523/JNEUROSCI.4247-12.2013

Baarendse, P. J. J., Van Grootheest, G., Jansen, R. F., Pieneman, A. W., Ogren, S. O., Verhage, M., et al. (2008). Differential involvement of the dorsal hippocampus in passive avoidance in C57bl/6J and DBA/2J mice. *Hippocampus* 18, 11–19. doi: 10.1002/hipo.20356

Bekkers, J. M., and Häusser, M. (2007). Targeted dendrotomy reveals active and passive contributions of the dendritic tree to synaptic integration and neuronal output. *Proc. Natl. Acad. Sci. U S A.* 104, 11447–11452. doi: 10.1073/pnas.0701546104

Bose, M., Muñoz-Llancao, P., Roychowdhury, S., Nichols, J. A., Jakkamsetti, V., Porter, B., et al. (2010). Effect of the environment on the dendritic morphology of the rat auditory cortex. *Synapse* 64, 97–110. doi: 10.1002/syn.20710

Brooks, S. P., Pask, T., Jones, L., and Dunnett, S. B. (2005). Behavioural profiles of inbred mouse strains used as transgenic backgrounds. II: cognitive tests. *Genes Brain Behav.* 4, 307–317. doi: 10.1111/j.1601-183X.2004.00109.x

Catapano, L. A., and Manji, H. K. (2007). G protein-coupled receptors in major psychiatric disorders. *Biochim. Biophys. Acta* 1768, 976–993. doi: 10.1016/j.bbamem.2006.09.025

Çetereisi, D., Kramvis, I., Gebuis, T., van der Loo, R. J., Gouwenberg, Y., Manvelder, H. D., et al. (2018). *Gpr158 Deficiency Impacts Hippocampal Ca1 Neuronal Excitability, Dendritic Architecture, and Affects Spatial Learning Biorxiv* [preprint] doi: 10.1101/506295

Chan, W. K. B., Zhang, H., Yang, J., Brender, J. R., Hur, J., Özgür, A., et al. (2015). GLASS: a comprehensive database for experimentally validated GPCR-ligand associations. *Bioinformatics* 31, 3035–3042. doi: 10.1093/bioinformatics/btv302

Condomitti, G., Wierda, K. D., Schroeder, A., Rubio, S. E., Vennekens, K. M., Orlandi, C., et al. (2018). An input-specific orphan receptor gpr158-hspg interaction organizes hippocampal mossy fiber-ca3 synapses. *Neuron* 100, 201.e–215.e. doi: 10.1016/j.neuron.2018.08.038

Dinocourt, C., Aungst, S., Yang, K., and Thompson, S. M. (2011). Homeostatic increase in excitability in area CA1 after schaffer collateral transection *in vivo*. *Epilepsia* 52, 1656–1665. doi: 10.1111/j.1528-1167.2011.03113.x

Elston, G. N., Benavides-Piccione, R., and DeFelipe, J. (2001). The pyramidal cell in cognition: a comparative study in human and monkey. *J. Neurosci.* 21:RC163.

Florian, C., and Roullet, P. (2004). Hippocampal CA3-region is crucial for acquisition and memory consolidation in Morris water maze task in mice. *Behav. Brain Res.* 154, 365–374. doi: 10.1016/j.bbr.2004.03.003

Fortune, E. S., and Rose, G. J. (2001). Short-term synaptic plasticity as a temporal filter. *Trends Neurosci.* 24, 381–385. doi: 10.1016/s0166-2236(00)01835-x

Goriounova, N. A., Heyer, D. B., Wilbers, R., Verhoog, M. B., Giugliano, M., Verbist, C., et al. (2018). Large and fast human pyramidal neurons associate with intelligence. *eLife* 7:e41714. doi: 10.7554/eLife.41714

Grant, S. G., O'Dell, T. J., Karl, K. A., Stein, P. L., Soriano, P., and Kandel, E. R. (1992). Impaired long-term potentiation, spatial learning, and hippocampal development in fyn mutant mice. *Science* 258, 1903–1910. doi: 10.1126/science.1361685

Hernández-Pérez, J. J., Gutiérrez-Guzmán, B. E., and Olvera-Cortés, M. E. (2016). Hippocampal strata theta oscillations change their frequency and coupling during spatial learning. *Neuroscience* 337, 224–241. doi: 10.1016/j.neuroscience.2016.09.003

Huang, Y., and Thathiah, A. (2015). Regulation of neuronal communication by G protein-coupled receptors. *FEBS Lett.* 589, 1607–1619. doi: 10.1016/j.febslet.2015.05.007

Khrimian, L., Obri, A., Ramos-Brossier, M., Rousseaud, A., Moriceau, S., Nicot, A.-S., et al. (2017). Gpr158 mediates osteocalcin's regulation of cognition. *J. Exp. Med.* 214:jem.20171320. doi: 10.1084/jem.20171320

Kowalski, J., Gan, J., Jonas, P., and Pernía-Andrade, A. J. (2016). Intrinsic membrane properties determine hippocampal differential firing pattern in vivo in anesthetized rats. *Hippocampus* 26, 668–682. doi: 10.1002/hipo.22550

Kulkarni, V. A., and Firestein, B. L. (2012). The dendritic tree and brain disorders. *Mol. Cell. Neurosci.* 50, 10–20. doi: 10.1016/j.mcn.2012.03.005

Leung, C. C. Y., and Wong, Y. H. (2017). Role of G protein-coupled receptors in the regulation of structural plasticity and cognitive function. *Molecules* 22:1239. doi: 10.3390/molecules22071239

Magee, J. C. (2000). Dendritic integration of excitatory synaptic input. *Nat. Rev. Neurosci.* 1, 181–190. doi: 10.1038/35044552

Mayford, M., Siegelbaum, S. A., and Kandel, E. R. (2012). Synapses and memory storage. *Cold Spring Harb. Perspect. Biol.* 4, a005751–a005751. doi: 10.1101/cshperspect.a005751

Micale, V., Stepan, J., Jurik, A., Pamplona, F. A., Marsch, R., Drago, F., et al. (2017). Extinction of avoidance behavior by safety learning depends on endocannabinoid signaling in the hippocampus. *J. Psychiatr. Res.* 90, 46–59. doi: 10.1016/j.jpsychires.2017.02.002

Mitsushima, D., Sano, A., and Takahashi, T. (2013). A cholinergic trigger drives learning-induced plasticity at hippocampal synapses. *Nat. Commun.* 4:2760. doi: 10.1038/ncomms3760

Mohan, H., Verhoog, M. B., Doreswamy, K. K., Eyal, G., Aardse, R., Lodder, B. N., et al. (2015). Dendritic and axonal architecture of individual pyramidal neurons across layers of adult human neocortex. *Cereb. Cortex* 25, 4839–4853. doi: 10.1093/cercor/bhv188

Myatt, D. R., Hadlington, T., Ascoli, G. A., and Nasuto, S. J. (2012). Neuromantic-from semi-manual to semi-automatic reconstruction of neuron morphology. *Front. Neuroinform.* 6:4. doi: 10.3389/fninf.2012.00004

Navakkode, S., Sajikumar, S., Korte, M., and Soong, T. W. (2012). Dopamine induces LTP differentially in apical and basal dendrites through BDNF and voltage-dependent calcium channels. *Learn. Mem.* 19, 294–299. doi: 10.1101/lm.026203.112

Okada, T., Yamada, N., Tsuzuki, K., Horikawa, H. P. M., Tanaka, K., and Ozawa, S. (2003). Long-term potentiation in the hippocampal CA1 area and dentate gyrus plays different roles in spatial learning. *Eur. J. Neurosci.* 17, 341–349. doi: 10.1046/j.1460-9568.2003.02458.x

Orlandi, C., Omori, Y., Wang, Y., Cao, Y., Ueno, A., Roux, M. J., et al. (2018). Transsynaptic binding of orphan receptor gpr179 to dystroglycan-pikachurin complex is essential for the synaptic organization of photoreceptors. *Cell Rep.* 25, 130–145.e5. doi: 10.1016/j.celrep.2018.08.068

Orlandi, C., Posokhova, E., Masuho, I., Ray, T. A., Hasan, N., Gregg, R. G., et al. (2012). GPR158/179 regulate G protein signaling by controlling localization and activity of the RGS7 complexes. *J. Cell Biol.* 197, 711–719. doi: 10.1083/jcb.201202123

Orlandi, C., Xie, K., Masuho, I., Fajardo-Serrano, A., Lujan, R., and Martemyanov, K. A. (2015). Orphan receptor GPR158 is an allosteric modulator of Regulator of G Protein Signaling 7 (RGS7) catalytic activity with essential role in dictating its expression and localization in the brain. *J. Biol. Chem.* 290, 13622–13639. doi: 10.1074/jbc.M115.645374

Ostrovskaya, O. I., Orlandi, C., Fajardo-Serrano, A., Young, S. M., Lujan, R., and Martemyanov, K. A. (2018). Inhibitory signaling to ion channels in hippocampal neurons is differentially regulated by alternative macromolecular complexes of RGS7. *J. Neurosci.* 38, 1318–1378. doi: 10.1523/JNEUROSCI.1378-18.2018

Patel, N., Itakura, T., Gonzalez, J. M., Schwartz, S. G., and Fini, M. E. (2013). GPR158, an orphan member of G protein-coupled receptor family C: glucocorticoid-stimulated expression and novel nuclear role. *PLoS One* 8:e57843. doi: 10.1371/journal.pone.0057843

Rao-Ruiz, P., Carney, K. E., Pandya, N., van der Loo, R. J., Verheijen, M. H. G., van Nierop, P., et al. (2015). Time-dependent changes in the mouse hippocampal synaptic membrane proteome after contextual fear conditioning. *Hippocampus* 25, 1250–1261. doi: 10.1002/hipo.22432

Rodgers, R. J., Boullier, E., Chatzimichalaki, P., Cooper, G. D., and Shorten, A. (2002). Contrasting phenotypes of C57BL/6JOlaHsd, 129S2/SvHsd and 129/SvEv mice in two exploration-based tests of anxiety-related behaviour. *Physiol. Behav.* 77, 301–310. doi: 10.1016/s0031-9384(02)00856-9

Schmitz, L. J. M., Klaassen, R. V., Ruiperez-Alonso, M., Zamri, A. E., Stroeder, J., Rao-Ruiz, P., et al. (2017). The AMPA receptor-associated protein Shisa7 regulates hippocampal synaptic function and contextual memory. *eLife* 6:e24192. doi: 10.7554/eLife.24192

Schroeder, A., Vanderlinden, J., Vints, K., Ribeiro, L. F., Vennekens, K. M., Gounko, N. V., et al. (2018). A Modular Organization of LRR Protein-Mediated synaptic adhesion defines synapse identity. *Neuron* 99, 329–344.e7. doi: 10.1016/j.neuron.2018.06.026

Scorcioni, R., Polavaram, S., and Ascoli, G. A. (2008). L-Measure: a web-accessible tool for the analysis, comparison and search of digital reconstructions of neuronal morphologies. *Nat. Protoc.* 3, 866–876. doi: 10.1038/nprot.2008.51

Spijker, S., Houtzager, S. W. J., De Gunst, M. C. M., De Boer, W. P. H., Schoffelmeer, A. N. M., and Smit, A. B. (2004). Morphine exposure and abstinence define specific stages of gene expression in the rat nucleus accumbens. *FASEB J.* 18, 848–850. doi: 10.1096/fj.03-0612fje

Spruston, N. (2008). Pyramidal neurons: dendritic structure and synaptic integration. *Nat. Rev. Neurosci.* 9, 206–221. doi: 10.1038/nrn2286

Sutton, L. P., Orlandi, C., Song, C., Oh, W. C., Muntean, B. S., Xie, K., et al. (2018). Orphan receptor GPR158 controls stress-induced depression. *eLife* 7:e33273. doi: 10.7554/eLife.33273

Tarantino, L. M., Gould, T. J., Druhan, J. P., and Bucan, M. (2000). Behavior and mutagenesis screens: the importance of baseline analysis of inbred strains. *Mamm. Genome* 11, 555–564. doi: 10.1007/s003350010107

Thakar, S., Wang, L., Yu, T., Ye, M., Onishi, K., Scott, J., et al. (2017). Evidence for opposing roles of Celsr3 and Vangl2 in glutamatergic synapse formation. *Proc. Natl. Acad. Sci. U.S.A.* 114, E610–E618. doi: 10.1073/pnas.1612062114

Thompson, M. D., Percy, M. E., McIntyre Burnham, W., and Cole, D. E. C. (2008). G protein-coupled receptors disrupted in human genetic disease. *Methods Mol. Biol.* 448, 109–137. doi: 10.1007/978-1-59745-205-2_7

Tronel, S., Fabre, A., Charrier, V., Oliet, S. H. R., Gage, F. H., and Abrous, D. N. (2010). Spatial learning sculpts the dendritic arbor of adult-born hippocampal neurons. *Proc. Natl. Acad. Sci. U S A.* 107, 7963–7968. doi: 10.1073/pnas.0914613107

Urrego, D., Troncoso, J., and Múnera, A. (2015). Layer 5 pyramidal neurons' dendritic remodeling and increased microglial density in primary motor cortex in a murine model of facial paralysis. *Biomed. Res. Int.* 2015:482023. doi: 10.1155/2015/482023

van Elburg, R. A. J., and van Ooyen, A. (2010). Impact of dendritic size and dendritic topology on burst firing in pyramidal cells. *PLoS Comput. Biol.* 6:e1000781. doi: 10.1371/journal.pcbi.1000781

Vetter, P., Roth, A., and Häusser, M. (2001). Propagation of action potentials in dendrites depends on dendritic morphology. *J. Neurophysiol.* 85, 926–937. doi: 10.1152/jn.2001.85.2.926

Võikar, V., Kõks, S., Vasar, E., and Rauvala, H. (2001). Strain and gender differences in the behavior of mouse lines commonly used in transgenic studies. *Physiol. Behav.* 72, 271–281. doi: 10.1016/s0031-9384(00)00405-4

Vorhees, C. V., and Williams, M. T. (2006). Morris water maze: procedures for assessing spatial and related forms of learning and memory. *Nat. Protoc.* 1, 848–858. doi: 10.1038/nprot.2006.116

Vuksic, M., Del Turco, D., Vlachos, A., Schuldt, G., Müller, C. M., Schneider, G., et al. (2011). Unilateral entorhinal denervation leads to long-lasting dendritic alterations of mouse hippocampal granule cells. *Exp. Neurol.* 230, 176–185. doi: 10.1016/j.expneurol.2011.04.011

Zucker, R. S., and Regehr, W. G. (2002). Short-term synaptic plasticity. *Annu. Rev. Physiol.* 64, 355–405. doi: 10.1146/annurev.physiol.64.092501.114547